JACS
JOURNAL OF THE AMERICAN CHEMICAL SOCIETY
pubs.acs.org/JACS
Article

Synthesis of Deuterated and Sulfurated Polymers by Inverse Vulcanization: Engineering Infrared Transparency via Deuteration

Munaum H. Qureshi, Jianhua Bao, Tristan S. Kleine, Kyung-Jo Kim, Kyle J. Carothers, Jake Molineux, Eunkyung Cho, Kyung-Seok Kang, Nicholas P. Godman, Veaceslav Coropceanu, Jean-Luc Bredas, Robert A. Norwood,* Jon T. Njardarson,* and Jeffrey Pyun*

Cite This: J. Am. Chem. Soc. 2023, 145, 27821−27829

Read Online

ACCESS | Metrics & More | Article Recommendations | Supporting Information

ABSTRACT: The synthesis of deuterated, sulfurated, proton-free, glassy polymers offers a route to optical polymers for infrared (IR) optics, specifically for midwave IR (MWIR) photonic devices. Deuterated polymers have been utilized to enhance neutron cross-sectional contrast with *proteo* polymers for morphological neutron scattering measurements but have found limited utility for other applications. We report the synthesis of perdeuterated d_{14}-(1,3-diisopropenylbenzene) with over 99% levels of deuteration and the preparation of proton-free, perdeuterated poly(sulfur-*random*-d_{14}-(1,3-diisopropenylbenzene)) (poly(S-*r*-d_{14}-DIB)) via inverse vulcanization with elemental sulfur. Detailed structural analysis and quantum computational calculations of these reactions demonstrate significant kinetic isotope effects, which alter mechanistic pathways to form different copolymer microstructures for *deutero* vs *proteo* poly(S-*r*-DIB). This design also allows for molecular engineering of MWIR transparency by shifting C−H bond vibrations around 3.3 μm/3000 cm^{-1} observed in *proteo* poly(S-*r*-DIB) to 4.2 μm/2200 cm^{-1}. Furthermore, the fabrication of thin-film MWIR optical gratings made from molding of deuterated-sulfurated, proton-free poly(S-*r*-d_{14}-DIB) is demonstrated; operation of these gratings at 3.39 μm is achieved successfully, while the *proteo* poly(S-*r*-DIB) gratings are opaque at these wavelengths, highlighting the promise of MWIR sensors and compact spectrometers from these materials.

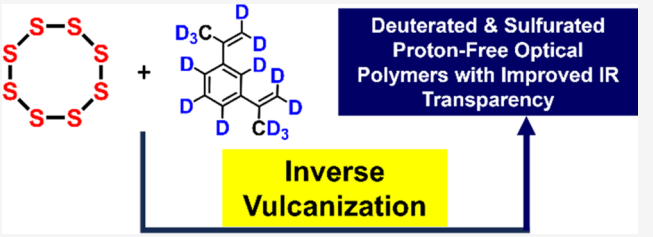

INTRODUCTION

The synthesis of deuterated molecules and materials is being widely studied for mass spectroscopic labeling, pharmaceuticals, and photonic devices.[1−6] In physical organic chemistry, deuterium labeling for mechanistic studies has long been known by exploiting kinetic isotope effects (KIE).[7,8] Furthermore, (per)deuterated synthetic macromolecules have been developed to enhance contrast for dimensional and morphological characterization of (co)polymers using neutron scattering techniques, most notably small angle neutron scattering (SANS).[9,10] Deuteration of polymers has been conducted for telecommunication photonics to reduce optical losses at 1310 nm.[3] However, wide-scale deployment of deuterated chemical and material products remains fairly limited in scope, pointing to the potential of new technologies exploiting the value of H/D exchange.

Synthetic methods to prepare deuterated molecules have focused on selective or partial deuteration of a target compound, with minimal examples of highly (per)deuterated molecules for pharmaceuticals. Deuteration methods require the use of heavy water (D_2O), molecular deuterium (D_2), or deuterated solvents as deuterium sources.[4,5,11] H/D exchange have been classically conducted in the presence of acid, base, and metal complexes for both homogeneous and heterogeneous processes.[1,2,4,5,12−14] Well-defined iridium-based catalysts have been used for deuteration of activated aromatic[13] vinylic C−H bonds[11,15] or nonactivated aliphatic C−H bonds with heterogeneous metal oxide catalysts.[5] More recent efforts have demonstrated selective isotopic labeling of bioactive molecules using the photoredox iridium catalysts of MacMillan et al.,[22] homogeneous iron catalysts for H/D exchange with D_2 gas by Chirik et al.,[23] and heterogeneous Fe(0)/FeC catalysts by Beller et al. using heavy water deuterium.[24] The synthesis of (per)deuterated polymers have primarily focused on a small subset of polymers (e.g., polystyrene, poly(methyl methacrylate), or polyethylene (PE)) for use in morphological SANS measurements, where deuteration is often conducted with D_2 and solid-supported rhodium[16] or platinum−rhenium alloyed supported catalysts[17−21] onto a polymeric substrate. More complex synthetic targets for deuteration require total synthesis approaches using perdeuterated starting materials,

Received: October 5, 2023
Revised: November 16, 2023
Accepted: November 17, 2023
Published: December 7, 2023

https://doi.org/10.1021/jacs.3c10985
J. Am. Chem. Soc. 2023, 145, 27821−27829

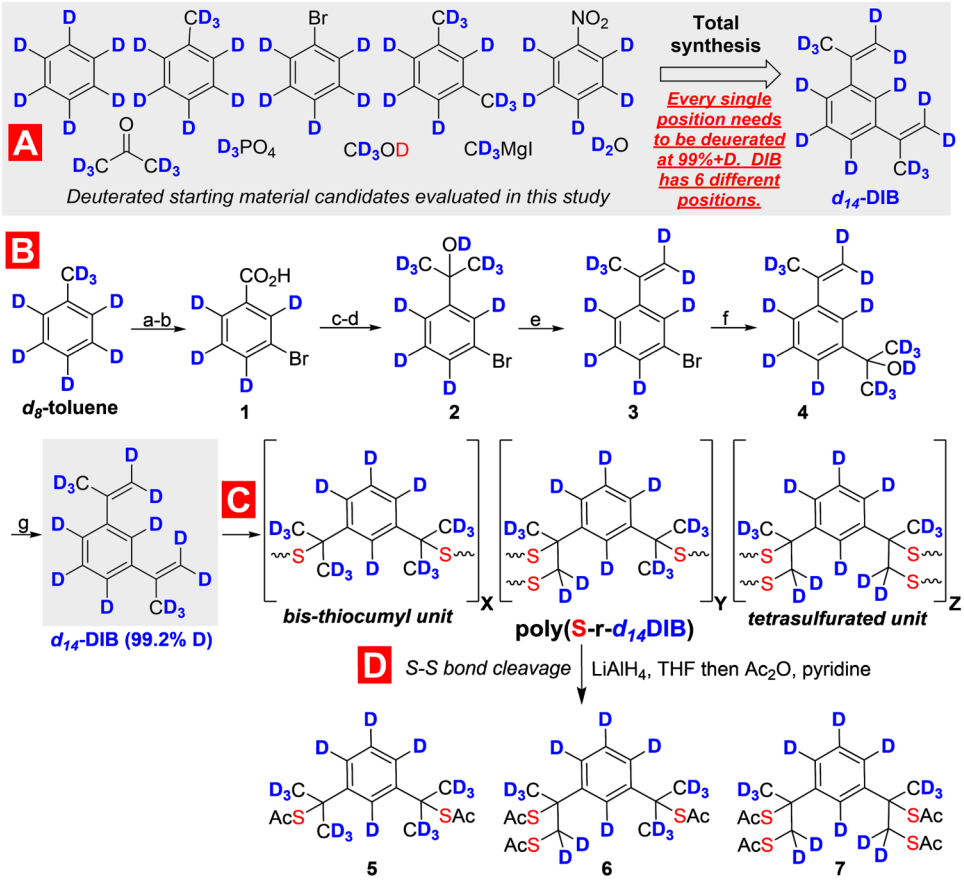

Figure 1. (A) Restricted suitable starting material selection and total synthesis challenges. (B) Total synthesis of d_{14}-DIB from d_8-toluene: (a) $KMnO_4$, Na_2CO_3, H_2O, 120 °C (54%); (b) $KBrO_3$, K_2SO_4, H_2O (94%); (c) MeOH, H_2SO_4 (86%); (d) CD_3MgI, Et_2O then CH_3OD (63%); (e) *p*-TsOD, benzene, 110 °C (53%); (f) *n*-BuLi, Et_2O, D_6-acetone, −78−0 °C, then CH_3OD (64%); (g) *p*-TsOD, benzene, 80 °C (54%). (C) Inverse vulcanization reaction of d_{14}-DIB with S_8 to prepare perdeuterated poly(S-*r*-d_{14}DIB) and (D) reductive polymer S−S bond degradation to determine the copolymer microstructure.

such as hexadeuterobenzene for the synthesis of perdeuterated α-methylstyrene.[25] Beers et al. developed an elegant synthesis of wholly or partially deuterated polyethylene(s)[26] beginning with NMR-grade deuterated solvents (d_6-DMSO, 99.9%) for the polyhomologation. However, the total synthesis of deuterated monomers of more complex architectures (e.g., *deutero*-substituted styrenics) has not widely been explored and poses significant synthetic challenges.

Deuteration holds intriguing possibilities for infrared (IR) optical polymers, particularly for the MWIR spectrum from 3 to 5 μm (or 3300−2000 cm^{-1}), where replacement of C−H for C−D bonds shifts and reduces the intensity of vibrational resonances from ∼3.3 μm (∼3000 cm^{-1}) to 4.2 μm (∼2200 cm^{-1}); this has also been highlighted in our recent computational work.[27] Synthetic polymers, particularly hydrocarbon-based materials, have had limited use for MWIR optical applications due to C−H bond vibrations in this spectral window, which has prompted the use of inorganic materials for these applications.[28] While H/D exchange does not completely remove MWIR absorbances outside the 3−5 μm spectrum, shifting of the vibrational resonance away from the 3.3 to 3.4 μm wavelength by replacing C−H with C−D bonds has significant utility given the importance of this spectral wavelength for chemical sensing and other emerging on-chip-miniaturized IR photonic devices.[29] Furthermore, spectral MWIR windows from ∼4.2 to 5.0 μm are rendered unusable for numerous MWIR optics and photonic applications (e.g., defense) because of carbon dioxide atmospheric absorption, further valorizing the MWIR window from 3.3 to 4.2 μm for application development. A breakthrough in polymer chemistry and optical sciences reported a decade ago was the inverse vulcanization polymerization of elemental sulfur (S_8) with *proteo*-1,3-diisopropenylbenzene (DIB), where the reduction of MWIR absorbing organic C−H bonds dramatically enhanced the IR transparency.[30−35] These hybrid polymers are analogous to inorganic chalcogenide glasses and hence have been referred to as chalcogenide hybrid inorganic/organic polymers (CHIPs) when used for optical applications.[28,36−46]

Herein, we report on the first total synthesis of perdeuterated 1,3-diisopropenylbenzene (d_{14}-DIB), copolymerization with elemental sulfur via inverse vulcanization, and MWIR optical device fabrication with these *perdeutero* chalcogenide hybrid copolymers. The current work is focused on the fundamental chemistry aspects of deuterated monomer synthesis and conducting the first IR optical structure−property comparison of *deutero* and *proteo* sulfurated copolymers. The emphasis of this study on the fundamental aspects of deuteration and sulfuration on IR transparency is a notable departure from the focus of S_8 utilization for polymer synthesis via inverse vulcanization. Prior emphasis in this field has been technologically focused on the production of high performance commodity polymers to enable consumption of

https://doi.org/10.1021/jacs.3c10985
J. Am. Chem. Soc. 2023, 145, 27821−27829

the enormous volume of S_8 produced from petroleum refining. Conversely, deuterated d_{14}-DIB was chosen as a challenging, esthetically appealing synthetic target to highlight how deceptively difficult it is to navigate this total synthesis with respect to selection of reactions and reaction order to realize 99%+ deuteration at all positions. While the multistep synthesis of this *deutero* monomer precludes use for commodity polymer applications, synthetic access to both *proteo* and *deutero*-DIB monomers allows for the interrogation of novel isotope effects on the inverse vulcanization polymerization, along with the comparative studies of *proteo* vs *deutero* poly(sulfur-*random*-(1,3-diisopropenylbenzene)) (poly(S-*r*-DIB)). In particular, the synthesis of both *proteo* and *deutero* poly(S-*r*-DIB) copolymers demonstrates the benefits of *deuteration and sulfuration* to engineer IR transparency as realized through the fabrication of IR polymer optical devices operating at 3.39 μm. This is the first demonstration of a functional IR optical element made from both *deuterated* and *sulfurated* polymers, opening up new technological possibilities for deuteration science and inverse vulcanization.

RESULTS AND DISCUSSION

Synthesis of d_{14}-DIB. Careful analysis of commercially available deuterated starting material candidates factoring in both price and deuterium enrichment levels (99%+) revealed only a handful of *deutero* aromatic precursors, along with deuterium oxide and acetone-d_6, that fit our synthetic criteria (Figure 1A). A number of different synthesis approaches were attempted but either led to undesirable H/D exchanges or challenges in accessing critical *deutero* reagents/intermediate products, which once again illustrated the major challenges encountered to synthesize fully deuterated target structures with high enrichment levels of deuterium at every position. For example, use of cross-couplings employing deuterated boron or stannane 2-propene groups were challenged by starting material syntheses, incomplete reactions, unacceptable H/D exchanges, and competing side reactions that resulted in additional obstacles in purifications.

The insights gained after several rounds of unsuccessful d_{14}-DIB total synthesis attempts enabled the design of a total synthesis of d_{14}-DIB with accessible deuterium-rich starting materials that negated the use of transition metals and employed steps to suppress hydrogen atom incorporation. Deuterated toluene (d_8-toluene) emerged as an optimal starting material, and strategies involving precise addition and elimination steps proved to be the most reliable in ensuring high deuterium incorporation throughout the total synthesis (Figure 1B). Toward that end, after oxidation[47] and bromination of d_8-toluene,[48] the resulting meta-bromo carboxylic acid **1** was esterified and subjected to CD_3MgI addition to afford **2**, following deuteration with CH_3OD. Dehydration was accomplished with deuterated *para*-toluenesulfonic acid (*p*-TsOD), yielding propene **3**. Transmetalation of the bromide and trapping of the resulting aryl lithium nucleophile with d_6-acetone delivered alcohol **4**. The final step in the total synthesis was dehydration with *p*-TsOD, which interestingly proceeded not only faster but also at lower temperatures than the earlier dehydration step. We were able to realize the first total synthesis of d_{14}-DIB with 99.2% deuterium incorporation, as evident from solution ^{13}C and ^{2}H NMR spectroscopy (Figure 2, see the Supporting Information, pg. S7, for details) and high-resolution mass spectrometry (see Figure S1). To our knowledge, this is the first ^{13}C NMR spectrum of a synthesized *deutero meta*-substituted styrenic monomer with only triplet resonances (since ^{2}H deuterons are spin +1 nuclei) observed for the deuterated carbon nuclei, which is only possible for very high levels of deuteration (Figure 2A). Solution ^{2}H NMR spectroscopy of the synthesized d_{14}-DIB is also striking evidence of successful deuteration (Figure 2C), where the chemical shifts of deuteron nuclei are near identical to the those of peaks from *proteo*-DIB from solution ^{1}H NMR spectroscopy (Figure 2D).

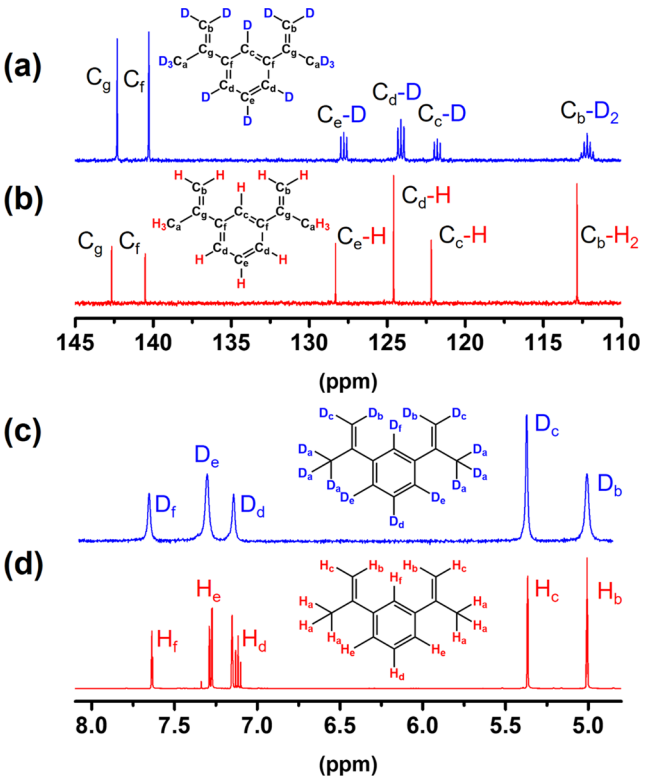

Figure 2. Solution ^{13}C NMR (in $CDCl_3$) spectra of (A) d_{14}-DIB (note only C, D carbons afford triplet peaks) and (B) *proteo*-DIB. (C) Solution ^{2}H NMR spectrum (in C_6D_6) of d_{14}-DIB. (D) Solution ^{1}H NMR (in C_6D_6) spectrum of *proteo*-DIB (ppm scales for all four spectra).

Synthesis of Perdeuterated Sulfur Copolymers via Inverse Vulcanization. With d_{14}-DIB in hand, the inverse vulcanization with S_8 was conducted (Figure 1C) with both 50 and 70 wt % sulfur feed ratios to prepare deuterated poly(S-*r*-d_{14}-DIB). Poly(S-*r*-d_{14}-DIB) with 50 wt % sulfur was solely used for fabrication of MWIR photonic devices as discussed below, since this copolymer composition afforded the most favorable melt processing characteristics and slightly higher glass transition vs high sulfur content copolymers. d_{14}-DIB was observed to be miscible in liquid sulfur at elevated temperatures (T = 165 °C) and produced orange glassy copolymers comparable to those of the *proteo* sulfur copolymers. Refractive index (n) characterization of both *proteo* and *deutero* sulfur copolymers was conducted via prism coupling (see Figure S21) with nearly identical values as the effects of H/D exchange are known to exhibit a negligible effect on n-values.[49] Thermal analysis using differential scanning calorimetry (DSC) and thermogravimetric analysis (TGA) confirmed a slight difference of a few degrees in the T_g values for the deuterated copolymers in comparison to *proteo* poly(S-*r*-DIB) 50/50

https://doi.org/10.1021/jacs.3c10985
J. Am. Chem. Soc. 2023, 145, 27821−27829

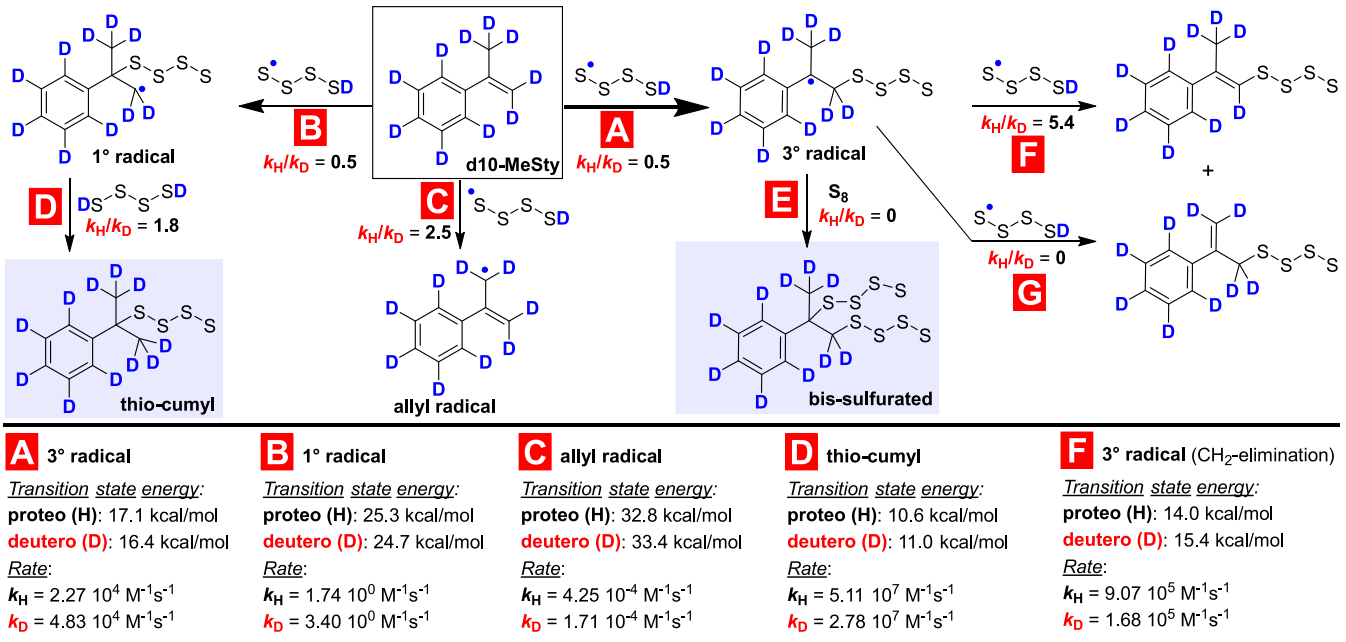

A 3° radical
Transition state energy:
proteo (H): 17.1 kcal/mol
deutero (D): 16.4 kcal/mol
Rate:
k_H = 2.27 10^4 $M^{-1}s^{-1}$
k_D = 4.83 10^4 $M^{-1}s^{-1}$

B 1° radical
Transition state energy:
proteo (H): 25.3 kcal/mol
deutero (D): 24.7 kcal/mol
Rate:
k_H = 1.74 10^0 $M^{-1}s^{-1}$
k_D = 3.40 10^0 $M^{-1}s^{-1}$

C allyl radical
Transition state energy:
proteo (H): 32.8 kcal/mol
deutero (D): 33.4 kcal/mol
Rate:
k_H = 4.25 10^{-4} $M^{-1}s^{-1}$
k_D = 1.71 10^{-4} $M^{-1}s^{-1}$

D thio-cumyl
Transition state energy:
proteo (H): 10.6 kcal/mol
deutero (D): 11.0 kcal/mol
Rate:
k_H = 5.11 10^7 $M^{-1}s^{-1}$
k_D = 2.78 10^7 $M^{-1}s^{-1}$

F 3° radical (CH_2-elimination)
Transition state energy:
proteo (H): 14.0 kcal/mol
deutero (D): 15.4 kcal/mol
Rate:
k_H = 9.07 10^5 $M^{-1}s^{-1}$
k_D = 1.68 10^5 $M^{-1}s^{-1}$

Figure 3. Calculated kinetic isotope effects from DFT for d_{10}-MeSty/Me-Sty model reactions with thiyl radicals to form observed thiocumyl and bis-sulfurated microstructures along with relevant competing reaction pathways.

composition ($T_{g\,proteo}$ = 29.7 °C, $T_{g\,deutero}$ = 23.6 °C, see Figure S3).

Structural Characterization of Poly(S-r-d_{14}-DIB). We recently reported that, in the inverse vulcanization of *proteo*-DIB with S_8, the copolymer microstructure is primarily a monosulfurated cumyl unit formed per olefinic group, in contrast to a bis-sulfurated microstructure from two C−S bonds formed per vinyl group as originally proposed.[50] Due to carbon-deuterium quadrupolar effects, solid-state ^{13}C NMR spectroscopic analysis of *deutero* poly(S-r-d_{14}-DIB) is not an accessible characterization technique. Hence, to interrogate the correct microstructure of *deutero* poly(S-*r*-DIB), structural analysis was conducted after reductive degradation of S−S bonds in the copolymer using $LiAlH_4$, followed by in situ acylation of thiols with *proteo* acetic anhydride, which facilitated recovery of the stable thioester degradation products. This reductive protocol was applied to both *proteo and deutero* poly(S-*r*-DIB) (50 and 70 wt % sulfur), which allowed for isolation of the three primary degradation products and comparisons of their relative ratios between (1) *proteo* and *deutero* and (2) weight %S on microstructure composition (our first NMR microstructural characterization of *proteo* poly(S-*r*-DIB) focused only on 50 wt % copolymer composition).[50] Isolation of the *proteo* and *deutero* thioacetate functional degradation products were conducted by silica gel chromatographic isolation of the degraded organosulfur units to enable structural identification of the *deutero* poly(S-*r*-d_{14}-DIB) copolymer microstructure using ^1H NMR spectroscopy. The acylation of degraded *deutero* units afforded *proteo*-thioacetate groups, which were used to quantify the copolymer microstructure. For the *proteo* poly(S-*r*-DIB), we observed that the bis-thiocumyl microstructure (50 mol %, X, 5, Figure 1C,D) was still the predominant copolymer unit; however, we also observed a minor microstructure unit with bis-sulfuration of olefins affording a tetrasulfurated microstructure unit (12.8 mol %), and a mixed microstructure unit with both thiocumyl and bis-sulfurated fragments. Most notably, the microstructure of the *deutero* poly(S-*r*-d_{14}-DIB) for both 50 and 70 wt % sulfur compositions exhibited significantly higher molar ratios of the tetrasulfurated microstructure (Z, 7, Figure 1C,D) and mixed cumyl/bis-sulfurated unit (Y, 6, Figure 1C,D) vs the *proteo* poly(S-*r*-DIB) due to isotope effects incurred in the inverse vulcanization (see the Supporting Information, Table S1 and Figures S4−S9).

Mechanistic Computational Calculations of the Isotope Effects during Inverse Vulcanization. These important differences in the microstructures of *proteo* vs *deutero* poly(S-*r*-DIB) and between 50 and 70 wt % sulfur compositions established from the degradation efforts prompted us to launch detailed computational studies using density functional theory calculations (DFT) as we reported previously for the *proteo*-DIB inverse vulcanization.[50] These calculations used tetrasulfane (H−S−S−S-S•) and α-methylstyrene (MeSty) as model compounds for the inverse vulcanization of S_8 and *proteo*-DIB. Summarized in Figure 3 are the key reactions (A−G) and the kinetic isotopic ratios ($k_{H/D}$) from these DFT calculations, which illustrate the pathways most affected by deuteration (see the Supporting Information, Figures S17−S20 for detailed results of the calculations). DFT calculations were carried out for the tetrasulfane thiyl radical addition to the less substituted carbon (Figure 3, A) or the more hindered carbon of d_{10}-MeSty/Me-Sty olefin (Figure 3, B), as well as for the competing allylic C−H/C−D abstraction pathway (Figure 3, C). As established from our earlier calculations, regiospecific thiol−ene pathway A to generate tertiary benzylic radicals is the preferred pathway and is 10^4 times faster than pathway B to generate primary radicals. The C−H/D allylic abstraction pathway C is 10^4 times slower than pathway B, although it is critical to emphasize that the retro-elimination reactions and the amount of sulfur used were shown to favor preferential formation of the 1° radical resulting in thiocumyl microstructures (Figure 3, D). The kinetic isotope effects for these competing pathways are most noteworthy, with both thiol−ene pathways (A and B) proceeding at a 2.0x faster rate for d_{10}-MeSty compared to *proteo* MeSty, with the less significant allylic abstraction pathway (C) favoring *proteo* MeSty.

https://doi.org/10.1021/jacs.3c10985
J. Am. Chem. Soc. 2023, 145, 27821−27829

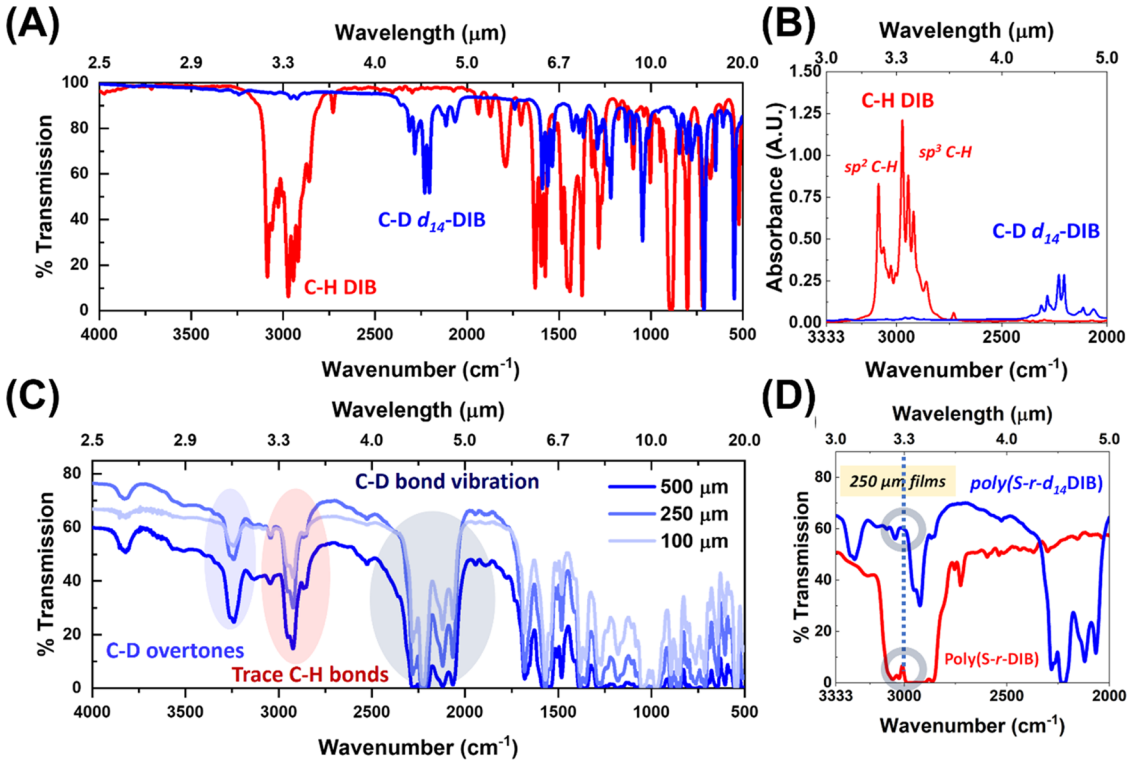

Figure 4. Stacked FTIR (A) transmission spectra of DIB (red) and d_{14}-DIB (blue) from 2.5 to 20 μm and (B) absorbance spectra DIB (red) and d_{14}-DIB (blue) from 3.0 to 5.0 μm. (C) Stacked transmission spectra of poly(S-*r*-d14-*DIB), 50* wt % S hot-pressed films of varying thickness from 100 to 500 μm. (D) Stacked IR transmission spectra of of *proteo* vs *deutero* poly(S-*r*-DIB) films (250 μm thick); the dashed line at 3.3 μm indicated a 60-fold difference in IR transmission between *proteo* and *deutero* poly(S-*r*-DIB).

Furthermore, *proteo* sulfane (H-SSSSH) termination of the 1° radical to form one of the primary thiocumyl microstructures (Figure 3, D) proceeds significantly faster (1.8×) for the *proteo* MeSty than for the *deutero* reaction pair, thus providing a route for the *deutero* radical elimination back to d_{10}-MeSty and for 3° radical formation en route to bis-sulfurated products. Formation of the bis-sulfurated product was calculated by ring-opening of S_8 with the 3° radical species, where the KIEs were negligible (Figure 3, E). It is important to note that of the two competing disproportionation pathways (Figure 3, F,G) on the *deutero* 3° radical, thiyl radical abstraction of methylene deuterium atoms (pathway F) was 5.4× slower than for the *proteo* reaction pair. Collectively, our DFT results on the possible KIE reactions confirm that for the *deutero* Me-Sty pathways, the generation of *deutero* tertiary radicals proceeds faster than for the *proteo* species (pathway A), and C, D thiyl radical abstraction is slower (5.4×) than the *proteo* species (pathway F), which then enhances the likelihood of the *deutero* 3° radical species to form the bis-sulfurated product in pathway E. Hence, from these DFT calculations, the enrichment in tetra- and bis-sulfurated microstructures (Figure 1, micro-structures Z, Y) of poly(S-*r*-d_{14}-DIB) can now be attributed to KIEs in the inverse vulcanization with d_{14}-DIB.

IR Spectroscopic Characterization of d_{14}-DIB and Poly(S-*r*-d_{14}-DIB). IR spectroscopy of d_{14}-DIB vs *proteo*-DIB was conducted with neat liquids drop cast between NaCl plates (effective thickness ≫50 μm) and demonstrated the differences between key vibrational C−H (3.3−3.4 μm) (~3000−2900 cm^{-1}) vs C−D bonds (2200−2000 cm^{-1}/4.2−5 μm) in the MWIR spectrum (Figure 4A,B, see the Supporting Information for details). The IR spectra of poly(S-*r*-d_{14}-DIB) (50 wt % sulfur) were taken on free-standing melt-processed films of varying thickness (from ~100 to 500 μm) and were found to be similar to those of the d_{14}-DIB monomer except for broadening of C−D fundamental vibrations from 2400 to 2000 cm^{-1}. A notable difference in the IR spectra of poly(S-*r*-d_{14}DIB) copolymer films vs drop cast d_{14}-DIB were two peaks around 2900 cm^{-1}/3.4 μm (from 0.8 mol % C−H in d_{14}-DIB, 99.2%) and 3250 cm^{-1}/3.1 μm (from C−D vibrational overtones). The IR spectra for thicker films revealed that the trace amount of *proteo* C−H bonds in the *deutero* poly(S-*r*-d_{14}-DIB) becomes more apparent at larger film thicknesses above 0.1 mm (see Figures 4C and S10 for full discussion). This corroborates the need for ultrahigh levels of purity (>99.99%) in IR inorganic semiconductors such as germanium to enable use for fabrication of free-standing lenses and windows exceeding 1 mm in thickness.[28] While it was evident from these studies on IR transmittance versus film thickness that bulk IR freeform optics exceeding 1 mm in thickness would require higher levels of deuteration in organic comonomers for inverse vulcanization, the benefits of deuteration in poly(S-*r*-d_{14}-DIB) were most evident in melt-pressed films at 250 μm. For such films, at the MWIR wavelengths of interest (3.3−3.4 μm), the IR transmittance of the *deutero* poly(S-*r*-DIB) was around 60-fold higher than the *proteo* poly(S-*r*-DIB) for 50 wt % sulfur compositions (Figure 4D). Hence, the opportunities to demonstrate the benefits of both deuteration and sulfuration in inversely vulcanized CHIPs for thin-film polymer MWIR photonics were investigated.

Design and Fabrication of MWIR Optical Grating from *Proteo* vs *Deutero* Poly(S-*r*-DIB). MWIR optical diffraction gratings were selected to highlight the benefits of sulfuration and deuteration in a moldable polymeric medium using a MWIR laser operating at 3.39 μm, comparing both

https://doi.org/10.1021/jacs.3c10985
J. Am. Chem. Soc. 2023, 145, 27821−27829

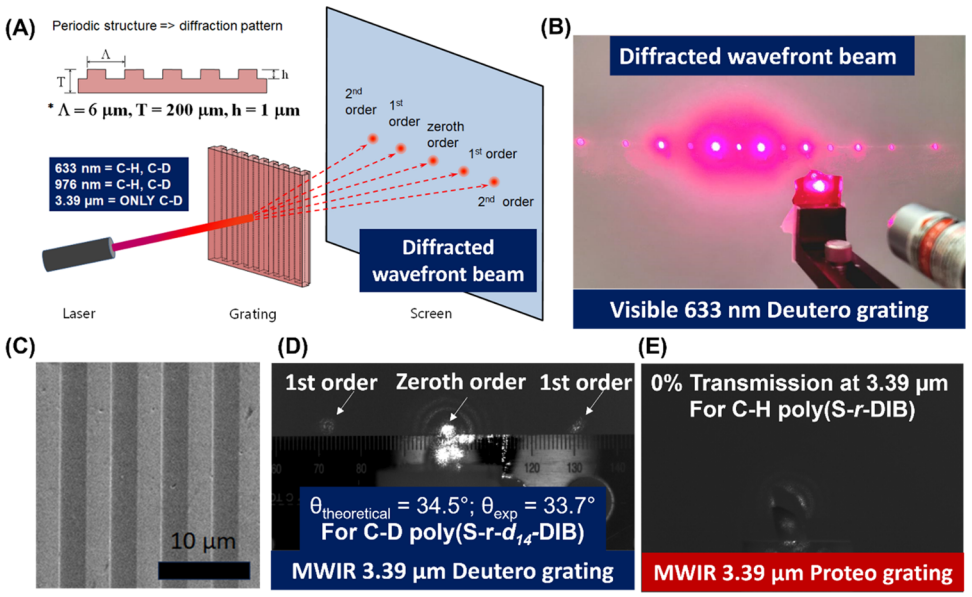

Figure 5. (A) Design of optical grating and schematic for diffraction grating experiment in the VIS−NIR−MWIR. (B) Optical diffracted beam through the poly(S-*r*-d_{14}-DIB) optical grating (total thickness = 250 μm with 50 μm flash layer) in the visible spectrum with 633 nm irradiation. (C) SEM image of poly(S-*r*-d_{14}-DIB) diffraction grating. (D) MWIR thermal image of 3.39 μm generated diffracted beam of zeroth and first orders through the poly(S-*r*-d_{14}-DIB) optical grating (total thickness = 250 μm). (E) Featureless MWIR image of 3.39 μm generated diffracted beam through the *proteo* poly(S-*r*-DIB) optical grating (total thickness = 250 μm, with a 50 μm flash layer).

proteo and *deutero* poly(S-*r*-DIB) composed of 50 wt % sulfur (see Figures S11 and S12 for design and fabrication details). The key demonstration is visualization of the MWIR diffracted wavefront pattern (see Figures 5A,B for diffracted beam examples) irradiated through a *deutero* poly(S-*r*-DIB) grating at MWIR wavelengths where the *proteo* diffractive grating is opaque. As shown in Figure 4D, this condition can be achieved for a 250 μm thick film of the poly(S-*r*-DIB) copolymer, for which the optical grating performance can be visualized by observing the various diffraction orders that occur at positions predicted by the grating eq (Figure S11). The periodicity of the gratings (6 μm end-wall to end-wall distance (Λ), 1 μm in height (h)) were chosen to maximize MWIR first-order diffraction spots due to the low intensity of MWIR photons and MWIR cameras used in this experiment (Figures 5A,B and S14 for details). To our knowledge, the fabrication of a MWIR polymeric optical grating has not been previously demonstrated. This particular MWIR experiment is particularly challenging because (1) MWIR laser sources operating near 3.3 μm are not widely available, (2) visualization of the MWIR diffracted wavefront pattern requires a MWIR thermal imaging camera, and (3) the majority of optical polymers contain C−H bonds that render the material opaque in the MWIR. For observation of the diffracted beams, both *proteo* and *deutero* poly(S-*r*-DIB) gratings were irradiated with 633 nm, 976 nm, and 3.39 μm monochromatic laser sources. As anticipated, these optical gratings performed identically in the visible spectrum at 633 nm (affording both low- and high-order diffraction spots, Figure 5B) and in the NIR at 976 nm (zeroth- and first-order spots projected onto the NIR card, see Figure S14). However, at 3.39 μm, only the *deutero* poly(S-*r*-DIB) optical grating produced a diffraction pattern with zeroth- and first-order MWIR spots (Figure 5D), whereas the *proteo* optical grating showed neither transmission nor diffraction (see Figure 5E) due to C−H bond vibrations in the polymeric medium. Furthermore, for the *deutero* poly(S-*r*-DIB) optical grating at 3.39 μm, the experimentally measured diffraction angle (θ_{exp} = 33.7°) was found to be in good agreement with the theoretical value ($\theta_{theoretical}$ = 34.5°) at 3.39 μm for the *deutero* poly(S-*r*-DIB) optical grating. Related work on the fabrication of MWIR polarizers from poly(S-*r*-DIB) has been reported,[51,52] with notable optical performance improvements by Cho et al.,[44] achieved through superior nanoimprint methods for MWIR polarizer fabrication.

CONCLUSIONS

The preparation of a new class of proton-free optical polymers is reported, which demonstrates the benefit of both *sulfuration* and *deuteration* to enable molecular engineering of IR transparency at the 3.3 μm/3300 cm^{-1} wavelength to enable MWIR photonics. The current report demonstrates numerous milestones toward this advance by the first total synthesis of perdeuterated d_{14}-(1,3-diisopropenylbenzene) at previously unattainable levels of deuteration (99%+) and application to the inverse vulcanization with S_8 to prepare deuterated poly(S-*r*-d_{14}-DIB). Detailed structural analysis and quantum computational calculations of the polymerization process demonstrate significant kinetic isotope effects which alter the mechanistic pathways to form different microstructures for *deutero* vs *proteo* poly(S-*r*-DIB). Finally, we fabricate thin-film optical diffraction gratings via polymer melt processing and molding of both *deutero* and *proteo* poly(S-*r*-DIB) where we demonstrate the benefits of deuteration to significantly improve IR transmittance (up to 60-fold enhancement of *deutero* vs *proteo* diffraction grating) and demonstrate MWIR imaging of the optical diffraction wavefront pattern in the MWIR spectrum. While the multistep synthesis of d_{14}-DIB using expensive deuterated starting materials precludes direct use for certain applications, this synthetic approach to proton-free, glassy, and moldable optical polymers holds significant potential for IR photonics as new, more cost-effective synthetic routes to deuterated monomers are developed. Furthermore, this

https://doi.org/10.1021/jacs.3c10985
J. Am. Chem. Soc. 2023, 145, 27821−27829

demonstration also opens new possibilities for deuteration chemistry to impact the fields of optical polymers and IR photonics.

EXPERIMENTAL METHODS

General Procedure Preparation of *Proteo* or *Deutero* Poly(S-*r*-DIB) with 50 wt % Sulfur. A Teflon-coated stir bar and sulfur (0.250 g, 7.8 mmol) were added to a small vial. The sulfur was heated in a silicone oil bath at 175 °C until the sulfur was melted and transparent, at which time DIB (0.250 g, 1.6 mmol) was added. The reaction was allowed to stir at 175 °C until the stir bar could no longer function due to the increased viscosity of the material. The reaction was further heated for 5 min at 175 °C to ensure completion of the polymerization. The vial was cooled to room temperature and then cooled in a dry ice/acetone bath. The vial was then broken to extract the dark red p(S-*r*-DIB). For the deuterated DIB samples, the same procedure was followed. However, it was observed that the point at which the stir bar stopped due to the viscosity of the reaction was several minutes faster, and the color of the product was significantly more orange.

General Procedure for Melt Processing of Optical Gratings from *Proteo* or *Deutero* Poly(S-*r*-DIB). An appropriate quantity of *proteo* poly(S-*r*-DIB) was placed in the hot-press between the two layers of the Kapton film. Using a 250 μm shim, the poly(S-*r*-DIB) was slowly pressed at 100 °C. The pressure was increased to 1 Ton, and the sample was held. at 100 °C for 10 min. The heat was then turned off, and the sample was allowed to cool to room temperature while still under pressure. The sample was then removed from the hot-press and the top Kapton film was removed. A previously prepared PDMS optical grating mold was added to the now exposed face of the sample, and it was placed back in the hot-press. The sample was heated to 100 °C, and the top plate of the press was lowered until it barely touched the PDMS mold (enough to provide heat transfer but not a significant amount of pressure). The sample remained at 100 °C for 20 min after which it was cooled to room temperature. Upon cooling to room temperature, the PDMS mold was carefully removed revealing the transferred optical grating pattern on the surface of the p(S-*r*-DIB) sample. For the *deutero* poly(S-*r*-DIB), the same process as for the *proteo* sample was used except a higher temperature (T = 150 °C) was employed.

ASSOCIATED CONTENT

Supporting Information

Table S1. The Supporting Information is available free of charge at https://pubs.acs.org/doi/10.1021/jacs.3c10985.

Full experimental and characterization details for Figures S1−S20; Table S1 (PDF)

AUTHOR INFORMATION

Corresponding Authors

Robert A. Norwood − *Wyant College of Optical Sciences, University of Arizona, Tucson, Arizona 85721, United States*; Email: rnorwood@optics.arizona.edu

Jon T. Njardarson − *Department of Chemistry and Biochemistry, University of Arizona, Tucson, Arizona 85721, United States*; orcid.org/0000-0003-2268-1479; Email: njardars@arizona.edu

Jeffrey Pyun − *Department of Chemistry and Biochemistry, University of Arizona, Tucson, Arizona 85721, United States; Wyant College of Optical Sciences, University of Arizona, Tucson, Arizona 85721, United States*; orcid.org/0000-0002-1288-8989; Email: jpyun@arizona.edu

Authors

Munaum H. Qureshi − *Department of Chemistry and Biochemistry, University of Arizona, Tucson, Arizona 85721, United States*

Jianhua Bao − *Department of Chemistry and Biochemistry, University of Arizona, Tucson, Arizona 85721, United States*

Tristan S. Kleine − *Department of Chemistry and Biochemistry, University of Arizona, Tucson, Arizona 85721, United States*

Kyung-Jo Kim − *Wyant College of Optical Sciences, University of Arizona, Tucson, Arizona 85721, United States*

Kyle J. Carothers − *Department of Chemistry and Biochemistry, University of Arizona, Tucson, Arizona 85721, United States; Air Force Research Laboratory, Materials and Manufacturing Directorate, Dayton, Ohio 45433, United States; Azimuth Corporation, Beavercreek, Ohio 45324, United States*

Jake Molineux − *Department of Chemistry and Biochemistry, University of Arizona, Tucson, Arizona 85721, United States*

Eunkyung Cho − *Department of Chemistry and Biochemistry, University of Arizona, Tucson, Arizona 85721, United States; Division of Energy Technology, DIGST, Daegu 42988, Republic of Korea*; orcid.org/0000-0001-8501-0029

Kyung-Seok Kang − *Department of Chemistry and Biochemistry, University of Arizona, Tucson, Arizona 85721, United States*

Nicholas P. Godman − *Air Force Research Laboratory, Materials and Manufacturing Directorate, Dayton, Ohio 45433, United States; Azimuth Corporation, Beavercreek, Ohio 45324, United States*; orcid.org/0000-0002-6801-309X

Veaceslav Coropceanu − *Department of Chemistry and Biochemistry, University of Arizona, Tucson, Arizona 85721, United States*; orcid.org/0000-0003-1693-2315

Jean-Luc Bredas − *Department of Chemistry and Biochemistry, University of Arizona, Tucson, Arizona 85721, United States*; orcid.org/0000-0001-7278-4471

Complete contact information is available at: https://pubs.acs.org/10.1021/jacs.3c10985

Author Contributions

All authors have given approval to the final version of the manuscript.

Notes

The authors declare the following competing financial interest(s): Robert A. Norwood is an owner and officer of Norcon Technologies Holding.

ACKNOWLEDGMENTS

The National Science Foundation and the Air Force Research Laboratories are gratefully acknowledged for support of this work through DMREF-2118578. We also acknowledge the National Science Foundation (PFI-RP 1940942, MRI-1920234), and the RII Research Advancement Grant program from the University of Arizona for supporting this work. The authors acknowledge funding from the Materials and Manufacturing Directorate of the Air Force Research Laboratory, Wright−Patterson Air Force Base, and the Organic Materials Chemistry Portfolio, Air Force Office of Science Research under contract #FA8650-16−D-5404. We thank Dr. Jixun Dai (University of Arizona, Department of Chemistry

and Biochemistry), Kathyrn P. Martin for assistance with polymer processsing, and Dr. Wallace Parker (ENI, s.P.A.) for assistance with NMR experiments.

REFERENCES

(1) Burwell, R. L. Deuterium as a tracer in reactions of hydrocarbons on metallic catalysts. *Acc. Chem. Res.* **1969**, *2*, 289−296.
(2) Atzrodt, J.; Derdau, V.; Kerr, W. J.; Reid, M. Deuterium- and Tritium-Labelled Compounds: Applications in the Life Sciences. *Angew. Chem., Int. Ed.* **2018**, *57*, 1758−1784.
(3) Ma, H.; Jen, A. K.-Y.; Dalton, L. R. Polymer-Based Optical Waveguides: Materials, Processing, and Devices. *Adv. Mater.* **2002**, *14*, 1339−1365.
(4) Kopf, S.; Bourriquen, F.; Li, W.; Neumann, H.; Junge, K.; Beller, M. Recent Developments for the Deuterium and Tritium Labeling of Organic Molecules. *Chem. Rev.* **2022**, *122*, 6634−6718.
(5) Sattler, A. Hydrogen/Deuterium (H/D) Exchange Catalysis in Alkanes. *ACS Catal.* **2018**, *8*, 2296−2312.
(6) Li, L.; Jakowski, J.; Do, C.; Hong, K. Deuteration and Polymers: Rich History with Great Potential. *Macromolecules* **2021**, *54*, 3555−3584.
(7) Westheimer, F. H. The Magnitude of the Primary Kinetic Isotope Effect for Compounds of Hydrogen and Deuterium. *Chem. Rev.* **1961**, *61*, 265−273.
(8) Gómez-Gallego, M.; Sierra, M. A. Kinetic Isotope Effects in the Study of Organometallic Reaction Mechanisms. *Chem. Rev.* **2011**, *111*, 4857−4963.
(9) Benoit, H.; Decker, D.; Higgins, J. S.; Picot, C.; Cotton, J. P.; Farnoux, B.; Jannink, G.; Ober, R. Dimensions of a Flexible Polymer Chain in the Bulk and in Solution. *Nat. Phys. Sci.* **1973**, *245*, 13−15.
(10) Bates, F. S.; Wignall, G. D.; Koehler, W. C. Critical Behavior of Binary Liquid Mixtures of Deuterated and Protonated Polymers. *Phys. Rev. Lett.* **1985**, *55*, 2425−2428.
(11) Zhou, J.; Hartwig, J. F. Iridium-Catalyzed H/D Exchange at Vinyl Groups without Olefin Isomerization. *Angew. Chem., Int. Ed.* **2008**, *47*, 5783−5787.
(12) Dixon, J. A.; Schiessler, R. W. Synthesis and Properties of Deuterocarbons. Benzene-d_6 and Cyclohexane-d_{12}[1a]. *J. Am. Chem. Soc.* **1954**, *76*, 2197−2199.
(13) Brown, W. G.; Garnett, J. L. Platinum-catalyzed Exchange of Aromatic Compounds with Deuterium Oxide. *J. Am. Chem. Soc.* **1958**, *80*, 5272−5274.
(14) Yung, C. M.; Skaddan, M. B.; Bergman, R. G. Stoichiometric and Catalytic H/D Incorporation by Cationic Iridium Complexes: A Common Monohydrido-Iridium Intermediate. *J. Am. Chem. Soc.* **2004**, *126*, 13033−13043.
(15) Camedda, N.; Serafino, A.; Maggi, R.; Bigi, F.; Cera, G.; Maestri, G. Functionalization of Alkenyl C−H Bonds with D2O via Pd(0)/Carboxylic Acid Catalysis. *Synthesis* **2020**, *52*, 1762−1772.
(16) Nicholson, J. C.; Crist, B. Hydrogen-deuterium exchange for labeling polyethylene. *Macromolecules* **1989**, *22*, 1704−1708.
(17) Habersberger, B. M.; Lodge, T. P.; Bates, F. S. Solvent Selective Hydrogen−Deuterium Exchange on Saturated Polyolefins. *Macromolecules* **2012**, *45*, 7778−7782.
(18) Habersberger, B. M.; Hart, K. E.; Gillespie, D.; Huang, T. Molecular Weight Dependence of Deuterium Exchange on Polyethylene: Direct Measurement and SANS Model. *Macromolecules* **2015**, *48*, 5951−5958.
(19) Zeng, Y.; López-Barrón, C. R.; Kang, S.; Eberle, A. P. R.; Lodge, T. P.; Bates, F. S. Effect of Branching and Molecular Weight on Heterogeneous Catalytic Deuterium Exchange in Polyolefins. *Macromolecules* **2017**, *50*, 6849−6860.
(20) Habersberger, B. M.; Baugh, D. W. Solvent and Polymer Stereochemistry Play Key Roles in Deuterium Exchange and Partial Racemization of Polypropylenes. *Macromolecules* **2018**, *51*, 1290−1295.
(21) Ertem, S. P.; Onuoha, C. E.; Wang, H.; Hillmyer, M. A.; Reineke, T. M.; Lodge, T. P.; Bates, F. S. Hydrogenolysis of Linear Low-Density Polyethylene during Heterogeneous Catalytic Hydrogen−Deuterium Exchange. *Macromolecules* **2020**, *53*, 6043−6055.
(22) Loh, Y. Y.; Nagao, K.; Hoover, A. J.; Hesk, D.; Rivera, N. R.; Colletti, S. L.; Davies, I. W.; MacMillan, D. W. C. Photoredox-catalyzed deuteration and tritiation of pharmaceutical compounds. *Science* **2017**, *358*, 1182−1187.
(23) Pony Yu, R.; Hesk, D.; Rivera, N.; Pelczer, I.; Chirik, P. J. Iron-catalysed tritiation of pharmaceuticals. *Nature* **2016**, *529*, 195−199.
(24) Li, W.; Rabeah, J.; Bourriquen, F.; Yang, D.; Kreyenschulte, C.; Rockstroh, N.; Lund, H.; Bartling, S.; Surkus, A.-E.; Junge, K.; Brückner, A.; Lei, A.; Beller, M. Scalable and selective deuteration of (hetero)arenes. *Nat. Chem.* **2022**, *14*, 334−341.
(25) Fetters, L. J.; Pummer, W. J.; Wall, L. A. Monomer-Polymer Equilibria of Deuterated α-Methylstyrenes. *J. Polym. Sci., Part A-1: Polym. Chem.* **1966**, *4*, 3003−3011.
(26) Farrell, W. S.; Orski, S. V.; Kotula, A. P.; Baugh III, D. W.; Snyder, C. R.; Beers, K. L. Precision, Tunable Deuterated Polyethylene via Polyhomologation. *Macromolecules* **2019**, *52*, 5741−5749.
(27) Cho, E.; Pratik, S. M.; Pyun, J.; Coropceanu, V.; Brédas, J.-L. π-Conjugated Carbon-Based Materials for Infrared Thermal Imaging. *Adv. Opt. Mater.* **2023**, *11*, No. 2300029.
(28) Kleine, T. S.; Glass, R. S.; Lichtenberger, D. L.; Mackay, M. E.; Char, K.; Norwood, R. A.; Pyun, J. 100th Anniversary of Macromolecular Science Viewpoint: High Refractive Index Polymers from Elemental Sulfur for Infrared Thermal Imaging and Optics. *ACS Macro Lett.* **2020**, *9*, 245−259.
(29) Sieger, M.; Mizaikoff, B. Toward On-Chip Mid-Infrared Sensors. *Anal. Chem.* **2016**, *88*, 5562−5573.
(30) Chung, W. J.; Griebel, J. J.; Kim, E. T.; Yoon, H.; Simmonds, A. G.; Ji, H. J.; Dirlam, P. T.; Glass, R. S.; Wie, J. J.; Nguyen, N. A.; Guralnick, B. W.; Park, J.; Somogyi, Á.; Theato, P.; Mackay, M. E.; Sung, Y.-E.; Char, K.; Pyun, J. The use of elemental sulfur as an alternative feedstock for polymeric materials. *Nat. Chem.* **2013**, *5*, 518−524.
(31) Griebel, J. J.; Glass, R. S.; Char, K.; Pyun, J. Polymerizations with elemental sulfur: A novel route to high sulfur content polymers for sustainability, energy and defense. *Prog. Polym. Sci.* **2016**, *58*, 90−125.
(32) Worthington, M. J. H.; Kucera, R. L.; Chalker, J. M. Green chemistry and polymers made from sulfur. *Green Chem.* **2017**, *19*, 2748−2761.
(33) Chalker, J. M.; Worthington, M. J. H.; Lundquist, N. A.; Esdaile, L. J. Synthesis and Applications of Polymers Made by Inverse Vulcanization. *Top Curr Chem (Z)* **2019**, *377*, 16.
(34) Zhang, Y.; Glass, R. S.; Char, K.; Pyun, J. Recent advances in the polymerization of elemental sulphur, inverse vulcanization and methods to obtain functional Chalcogenide Hybrid Inorganic/Organic Polymers (CHIPs). *Polym. Chem.* **2019**, *10*, 4078−4105.
(35) Lee, T.; Dirlam, P. T.; Njardarson, J. T.; Glass, R. S.; Pyun, J. Polymerizations with Elemental Sulfur: From Petroleum Refining to Polymeric Materials. *J. Am. Chem. Soc.* **2022**, *144*, 5−22.
(36) Griebel, J. J.; Namnabat, S.; Kim, E. T.; Himmelhuber, R.; Moronta, D. H.; Chung, W. J.; Simmonds, A. G.; Kim, K.-J.; van der Laan, J.; Nguyen, N. A.; Dereniak, E. L.; Mackay, M. E.; Char, K.; Glass, R. S.; Norwood, R. A.; Pyun, J. New Infrared Transmitting Material via Inverse Vulcanization of Elemental Sulfur to Prepare High Refractive Index Polymers. *Adv. Mater.* **2014**, *26*, 3014−3018.
(37) Anderson, L. E.; Kleine, T. S.; Zhang, Y.; Phan, D. D.; Namnabat, S.; LaVilla, E. A.; Konopka, K. M.; Ruiz Diaz, L.; Manchester, M. S.; Schwiegerling, J.; Glass, R. S.; Mackay, M. E.; Char, K.; Norwood, R. A.; Pyun, J. Chalcogenide Hybrid Inorganic/Organic Polymers: Ultrahigh Refractive Index Polymers for Infrared Imaging. *ACS Macro Lett.* **2017**, *6*, 500−504.
(38) Boyd, D. A.; Baker, C. C.; Myers, J. D.; Nguyen, V. Q.; Drake, G. A.; McClain, C. C.; Kung, F. H.; Bowman, S. R.; Kim, W.; Sanghera, J. S. ORMOCHALCs: organically modified chalcogenide polymers for infrared optics. *Chem. Commun.* **2017**, *53*, 259−262.

https://doi.org/10.1021/jacs.3c10985
J. Am. Chem. Soc. 2023, 145, 27821−27829

(39) Kleine, T. S.; Diaz, L. R.; Konopka, K. M.; Anderson, L. E.; Pavlopolous, N. G.; Lyons, N. P.; Kim, E. T.; Kim, Y.; Glass, R. S.; Char, K.; Norwood, R. A.; Pyun, J. One Dimensional Photonic Crystals Using Ultrahigh Refractive Index Chalcogenide Hybrid Inorganic/Organic Polymers. *ACS Macro Lett.* **2018**, *7*, 875−880.
(40) Boyd, D. A.; Nguyen, V. Q.; McClain, C. C.; Kung, F. H.; Baker, C. C.; Myers, J. D.; Hunt, M. P.; Kim, W.; Sanghera, J. S. Optical Properties of a Sulfur-Rich Organically Modified Chalcogenide Polymer Synthesized via Inverse Vulcanization and Containing an Organometallic Comonomer. *ACS Macro Lett.* **2019**, *8*, 113−116.
(41) Kleine, T. S.; Lee, T.; Carothers, K. J.; Hamilton, M. O.; Anderson, L. E.; Ruiz Diaz, L.; Lyons, N. P.; Coasey, K. R.; Parker Jr, W. O.; Borghi, L.; Mackay, M. E.; Char, K.; Glass, R. S.; Lichtenberger, D. L.; Norwood, R. A.; Pyun, J. Infrared Fingerprint Engineering: A Molecular-Design Approach to Long-Wave Infrared Transparency with Polymeric Materials. *Angew. Chem., Int. Ed.* **2019**, *58*, 17656−17660.
(42) Lee, J. M.; Noh, G. Y.; Kim, B. G.; Yoo, Y.; Choi, W. J.; Kim, D.-G.; Yoon, H. G.; Kim, Y. S. Synthesis of Poly(phenylene polysulfide) Networks from Elemental Sulfur and p-Diiodobenzene for Stretchable, Healable, and Reprocessable Infrared Optical Applications. *ACS Macro Lett.* **2019**, *8*, 912−916.
(43) Nishant, A.; Kim, K.-J.; Showghi, S. A.; Himmelhuber, R.; Kleine, T. S.; Lee, T.; Pyun, J.; Norwood, R. A. High Refractive Index Chalcogenide Hybrid Inorganic/Organic Polymers for Integrated Photonics. *Adv. Opt. Mater.* **2022**, *10*, No. 2200176.
(44) Cho, W.; Hwang, J.; Lee, S. Y.; Park, J.; Han, N.; Lee, C. H.; Kang, S.-W.; Urbas, A.; Kim, J. O.; Ku, Z.; Wie, J. J. Highly Sensitive and Cost-Effective Polymeric-Sulfur-Based Mid-Wavelength Infrared Linear Polarizers with Tailored Fabry−Pérot Resonance. *Adv. Mater.* **2023**, *35*, No. 2209377.
(45) Hwang, J. H.; Kim, S. H.; Cho, W.; Lee, W.; Park, S.; Kim, Y. S.; Lee, J.-C.; Lee, K. J.; Wie, J. J.; Kim, D.-G. A Microphase Separation Strategy for the Infrared Transparency-Thermomechanical Property Conundrum in Sulfur-Rich Copolymers. *Adv. Opt. Mater.* **2023**, *11*, No. 2202432.
(46) Lee, M.; Oh, Y.; Yu, J.; Jang, S. G.; Yeo, H.; Park, J.-J.; You, N.-H. Long-wave infrared transparent sulfur polymers enabled by symmetric thiol cross-linker. *Nat. Commun.* **2023**, *14*, 2866.
(47) Shi, W.-Y.; Ding, Y.-N.; Zheng, N.; Gou, X.-Y.; Zhang, Z.; Chen, X.; Luan, Y.-Y.; Niu, Z.-J.; Liang, Y.-M. Highly regioselective and stereoselective synthesis of C-Aryl glycosides via nickel-catalyzed ortho-C−H glycosylation of 8-aminoquinoline benzamides. *Chem. Commun.* **2021**, *57*, 8945−8948.
(48) Groweiss, A. Use of Sodium Bromate for Aromatic Bromination: Research and Development. *Org. Process Res. Dev.* **2000**, *4*, 30−33.
(49) Kaino, T.; Jinguji, K.; Nara, S. Low loss poly-(methylmethacrylate-d8) core optical fibers. *Appl. Phys. Lett.* **1983**, *42*, 567−569.
(50) Bao, J.; Martin, K. P.; Cho, E.; Kang, K.-S.; Glass, R. S.; Coropceanu, V.; Bredas, J.-L.; Parker, W. O. N., Jr; Njardarson, J. T.; Pyun, J. On the Mechanism of the Inverse Vulcanization of Elemental Sulfur: Structural Characterization of Poly(sulfur-random-(1,3-diisopropenylbenzene)). *J. Am. Chem. Soc.* **2023**, *145*, 12386−12397.
(51) Islam, M. D.; Kim, J. O.; Ko, Y.; Ku, Z.; Boyd, D. A.; Smith, E. M.; Nguyen, V. Q.; Myers, J. D.; Baker, C. C.; Kim, W.; Sanghera, J. S.; Czaplewski, D. A.; Urbas, A. M.; Genzer, J.; Ryu, J. E. Design of High Efficient Mid-Wavelength Infrared Polarizer on ORMOCHALC Polymer. *Macromol. Mater. Eng.* **2020**, *305*, No. 2000033.
(52) Islam, M. D.; Liu, S.; Derov, J.; Urbas, A. M.; Ku, Z.; Sihn, A.; Smith, E. M.; Boyd, D. A.; Kim, W.; Sanghera, J. S.; Nguyen, V. Q.; Myers, J. D.; Baker, C. C.; Ryu, J. E. *IMECol.3V* 2021; Vol. 3.

https://doi.org/10.1021/jacs.3c10985
J. Am. Chem. Soc. 2023, 145, 27821−27829